When a crack is oriented by a magnetic field

L. Pauchard,[1,2] F. Elias,[1,3,*] P. Boltenhagen,[1] A. Cebers,[1,4] and J. C. Bacri[1]
[1]*Laboratoire Matière et Systèmes Complexes, Universitè Paris 7, CNRS UMR 7057, France*
[2]*Laboratoire Fluides, Automatique et Systèmes Thermiques, Universitè Pierre et Marie Curie–Paris 6, Universitè Paris-Sud, CNRS, F-91405, France*
and Laboratoire FAST, Batiment 502, Campus Universitè, Orsay, F-91405, France
[3]*Physics Department, Universitè Paris 6, UFR 925, 4 Place Jussieu, 75252 Paris Cedex 05, France*
[4]*Institute of Physics, Mieraiela 32, Salaspils, LV 2169 Latvia*
(Received 6 September 2007; published 12 February 2008)

Upon drying, colloidal suspensions undergo a phase transformation from a "liquid" to a "gel" state. With further solvent evaporation, tensile stresses develop in the gel, which ultimately leads to fractures. These generally manifest themselves in regular cracking patterns which reflect the physical conditions of the drying process. Here we show experimentally and theoretically how, in the case of a drying droplet of magnetic colloid (ferrofluid), an externally applied magnetic field modifies the stress in the gel and therefore the crack patterns. We find that the analysis of the shape of the cracks allows one to estimate the value of the gel Young's modulus just before the crack nucleation.

DOI: 10.1103/PhysRevE.77.021402 PACS number(s): 83.80.Hj, 62.20.M−, 47.54.−r

I. INTRODUCTION

The crack patterns formed during the drying of pastes have been the subject of many investigations. The application of such studies is very wide—for instance, in the drying of paint in industry [1,2] or in the arts [3]. Many coating and material elaboration processes are also based on the drying of colloidal suspensions, where cracking needs to be avoided [4]. Understanding the crack patterns of muddy sediments has also a geological interest [5].

The fundamental interest in the study of the drying process of colloidal suspensions is the link between the microscopic interactions between the colloidal particles during solvent evaporation and the macroscopic morphology and geometry of the resulting crack pattern. Under well-controlled experimental conditions, a regular crack pattern can be formed during the drying process, the cracks being regularly spaced and perpendicular to the gelation front [6–9].

In this article, we study the drying of a colloidal suspension made of magnetic particles (ferrofluid). The presence of an external magnetic field in the plane of the substrate induces an additional anisotropic interaction between the particles. The macroscopic effect is spectacular: the cracks propagating in the gel phase turn and align in the same direction as the magnetic field, as shown in Fig. 1.

The article is organized as follows. We first recall the mechanism of crack patterns in nonmagnetic colloidal suspension and introduce the vocabulary and the notations (Sec. II). We then present the experimental setup (Sec. III). The experimental procedure and results are shown in Sec. IV. In Sec. V, we introduce a model that takes into account the magnetic-dipole interaction within the drying ferrofluid drop submitted to an external magnetic field. Those interactions induce a magnetic stress, which acts on the crack during the crack propagation. The shape of the crack is then fixed by the interplay between the elastic and magnetic stresses. We compute the exact shape of the crack as a function of the external field and show that this model reproduces well the experimental data (Sec. VI). We finally discuss (Sec. VII) and conclude (Sec. VIII) this study.

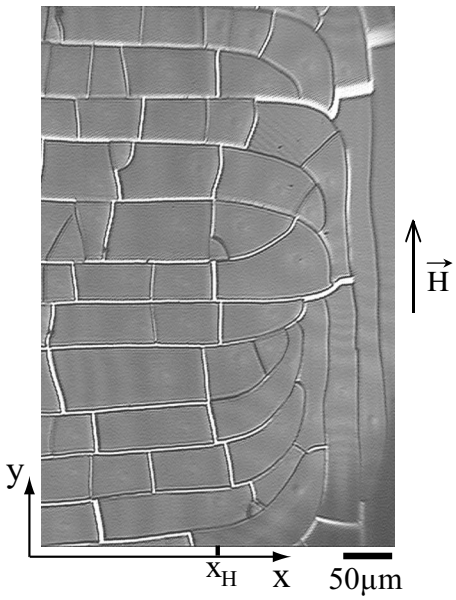

FIG. 1. Region of a ferrofluid drop in the final stage of the drying process. The direction of propagation of the gelation front was along the x axis. The drop started to dry in the absence of external magnetic field (left part). A homogeneous magnetic field of amplitude $H=16$ kA m^{-1} was then applied in the direction of the y axis when the gelation was at the position $x=x_H$. From the left to the right of the figure, the cracks turn in order to align in the same direction as the magnetic field.

*elias@ccr.jussieu.fr

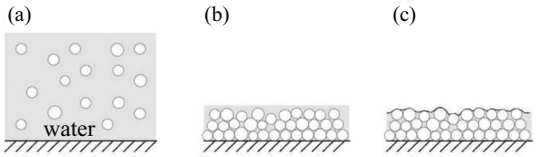

FIG. 2. Sketch of the drying process of a colloidal suspension. Because of the solvent evaporation, the stable colloid (a) transits to a gel phase when the particles come into contact (b). The water evaporation then causes liquid bridges between the particles, which are at the origin of growing tensile stress into the gel phase (see text).

II. CRACK PATTERNS WITHOUT A MAGNETIC FIELD

Controlling the crack path is very important in various fields of science and technology. Such a control has been proven to be possible if the colloid is confined between two glass plates by changing the cooling rate during quenching [10,11]. More recently, experiments involving vibrating pastes were performed to mechanically control the crack patterns that appear during the drying process of a drop deposited onto a glass plate [12].

The crack mechanism in drying colloidal suspensions has been understood as follows [4,13]. Let us consider a liquid drop of a colloidal aqueous suspension on a substrate (see Fig. 2). During the water evaporation, the distance between particles decreases, until the particles enter in contact. At this point, the system consists in a porous structure saturated with the solvent [Fig. 2(b)], which we call alternatively the *gel phase* or *paste*. After this gel phase is formed, the water goes on evaporating between the particles [Fig. 2(c)]. The particles interact under the effect of capillary bridges. Therefore, the gel shrinks due to high capillary pressure, which is of the order of $2\gamma_{w,a}/a \approx 10^7$ Pa, where $\gamma_{w,a}$ is the water-air surface tension and a is the average particle radius. But the gel shrinkage is limited by the adhesion on the substrate. As a result of this growing misfit, mechanical tensile stresses build up within the gel. The tensile stress increases with the increase of the solvent evaporation. When the stress reaches a critical value, cracks nucleate from defects in the system and invade the gel [6].

The stress tensor within the gel is usually anisotropic, and the cracks propagate in the direction that relaxes the highest stress—i.e., perpendicularly to the direction of maximal stress. In the geometry of a sessile droplet, the drying starts at the edge of the droplet and propagates toward the center (see Fig. 3 and Ref. [8]). Directional cracks are then formed at the edge of the drop (near the three-phase line) and propagate radially as the gel phase extends from the periphery to the center of the drop. A pattern of regularly spaced cracks builds up all around the drop edge. Figure 3 shows that, when the droplet is observed in the plane of the substrate, two propagation fronts can clearly be defined. We introduce the following notations. The x axis is the direction of propagation of the drying process. The x axis is then radially oriented from the edge to the center of the drop. The *gelation front* is the line separating the liquid phase and the gel phase. Note that, in the experiments, the liquid and solid phases are

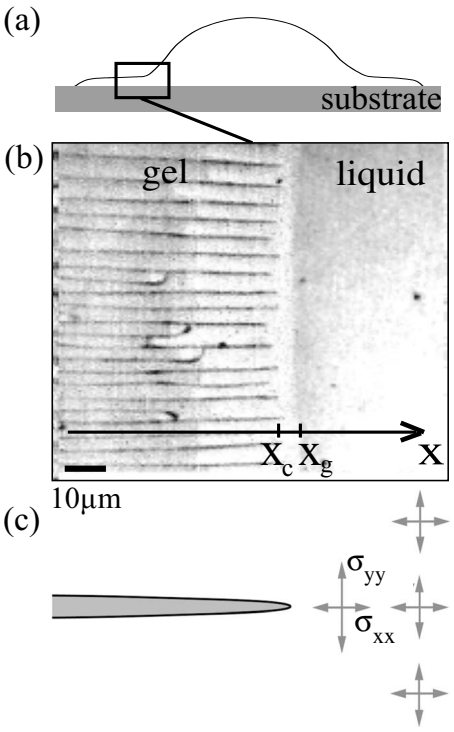

FIG. 3. (a) Sketch of a sessile drop in side view, drying on a substrate (a glass plate): a gelled foot builds up near the drop edge while the central part is still fluid and shrinks. (b) Photograph of the top view of a section of a drying drop. A pattern of cracks builds up all around the drop edge: x_c and x_g denote the positions of the cracking and gelation front, respectively. The black bar represents 10 μm. (c) Sketch of the growth of a crack in the stretched gel phase corresponding to the left part of image (b). $\sigma_{yy} > \sigma_{yy}$ is the maximum stress; therefore, the fracture opens in the direction perpendicular to the y axis.

clearly distinguished by the presence of impurities (dust): the impurities constantly move in the liquid phase whereas they are blocked in the gel phase. In the gel phase, the tips of the cracks are aligned on a line parallel to the gelation front. We call this line the *cracking front*. x_g is the position of the gelation front on the x axis, and x_c is the position of the cracking front.

III. EXPERIMENTAL SETUP

The drying drops studied in this article are made of a ferrofluid, which is a stable colloidal suspension of magnetic particles in a solvent. In our case it is a dispersion of maghemite (γ-Fe_2O_3) particles in water (volume fraction $\phi_{FF}=2.1\%$, average particle diameter $\langle 2a \rangle = 10$ nm, particle diameter lying between $2a=3$ nm and $2a=15$ nm). The ferrofluid is stabilized electrostatically by a negative surface charge of the particles (citrate ions adsorbed on the surface of the particles). The solution is electrically neutralized by sodium counter-ions [14]. The suspension is stable in the absence of solvent evaporation.

Each particle carries a permanent magnetic moment, conferring macroscopic magnetic properties to the solution

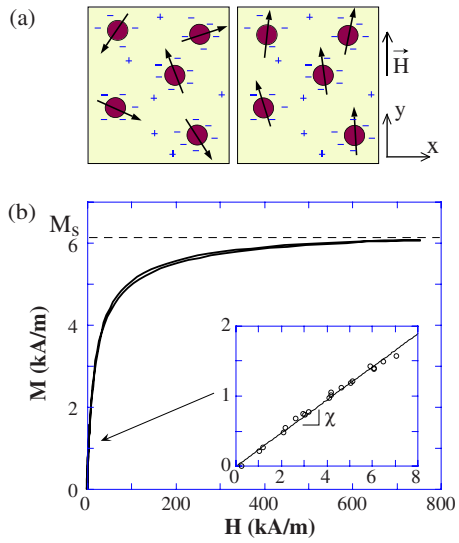

FIG. 4. (Color online) (a) Sketch of an ionic ferrofluid. The average particle diameter is $\langle 2a \rangle = 10$ nm. In the absence of an applied magnetic field, the magnetic moments of the particles are randomly oriented because of the Brownian motion, whereas they are aligned under the effect of an applied magnetic field. (b) Magnetization curve of the ferrofluid used in the experiments. The inset shows the linear range of the magnetization curve, in which the initial magnetic susceptibility of the ferrofluid is measured. The magnetic susceptibility is $\chi = 0.23$, and the saturation magnetization is $M_s = 6.7$ kA m^{-1}

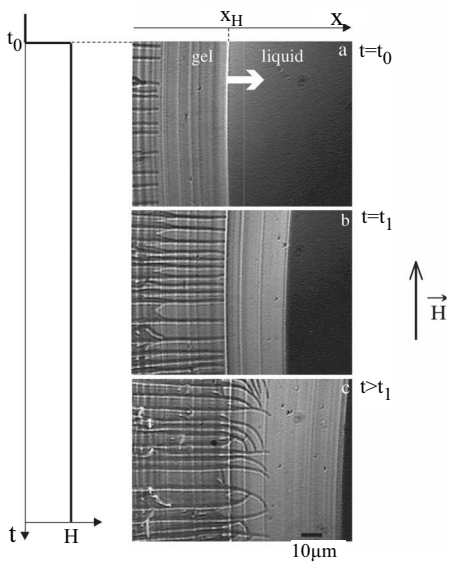

FIG. 5. Propagation of the gel phase and the cracks in a drying ferrofluid drop. (a) At $t = t_0$, a magnetic field $H = 25$ kA m^{-1} is applied in the y direction (no magnetic field is applied for $t < t_0$). (b) At $t = t_1$, the cracking front x_c reaches the position where the gelation front x_g was when the magnetic field was switched on: $x_c(t_1) = x_g(t_0) = x_H$. (c) At $t > t_1$, the crack trajectories are bent increasingly toward the direction of the applied field. Let us notice that in the top of the image, the cracks turn clockwise, whereas they are more likely to turn counterclockwise in the bottom of the image. This effect is due to the circular geometry of the gelation front, which orientates the crack radially in the absence of a magnetic field: only in the middle of the figure is the initial crack direction strictly perpendicular to the field.

(Fig. 4). In the presence of an external magnetic field, thermal agitation competes with the magnetic energy, which tends to align the magnetic moments of the particles in the same direction as the external field [15–17]. The resulting macroscopic magnetic behavior of the solution is of paramagnetic type: the magnetization $\vec{M}(\vec{H})$ of the ferrofluid has the same direction as the applied field $\vec{H}$; the amplitude $M(H)$ increases linearly with the external field for low field strength and saturates for high applied magnetic field strength since all the magnetic dipoles are aligned. Figure 4(b) shows the magnetization curve of the ferrofluid solution used in the experiments (before the drying).

A small amount of the solution (around 20 μl) is deposited on a horizontal glass plate, forming a hemispherical droplet which is bounded by a three-phase contact line on the glass plate [18]. During the water evaporation, the liquid suspension transits to a gel phase, which propagates as a so-called gelation front from the periphery of the drop to its center. The drop diameter is of the order of 5 mm; its height is of the order of 3 mm in the liquid phase and of 100 μm in the gel phase.

The sessile droplet is placed between Helmholtz coils, which create a homogeneous magnetic field in the plane of the glass plate. The amplitude of the magnetic field can be varied between 0 and 25 kA m^{-1}. The morphology of the drying drop and the crack pattern are imaged from the top using a microscope and a camera.

IV. EXPERIMENTAL RESULTS

The propagation of the cracks during the drying process of a ferrofluid drop, with or without a magnetic field, is shown in Fig. 5. The geometry is the same as in Fig. 3: the drop, initially hemispherical, dries from the circular edge toward the center. The images are top views of a portion of the drop. They show the gelation front and the cracking front on a distance of approximately 0.3% of their total length: at this scale, the gelation and cracking fronts appear linear. In this region, the gelation front propagates perpendicularly to the applied magnetic field. The ferrofluid drop is deposited on the substrate at $t = 0$.

Between time $t = 0$ and $t = t_0$, no magnetic field is applied. A gelation front propagates from the edge to the center of the drop in the x direction, followed by a crack front propagating in the same direction. As in the case of the drying process of a nonmagnetic colloidal suspension, the cracks are regularly spaced and aligned in the direction perpendicular to the gelation front.

At $t = t_0$, the external homogeneous magnetic field $\vec{H}$ is applied in the y direction. The cracks go on propagating in the x direction until $t = t_1$, when the cracking front reaches the position that was the position of the gelation front at the time the magnetic field was switched on [Fig. 5(b)]: $x_c(t_1) = x_g(t_0) = x_H$.

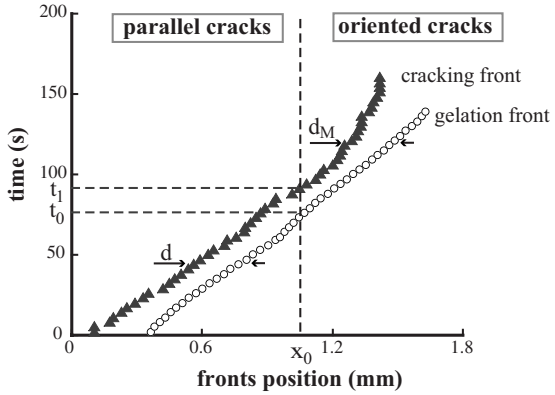

FIG. 6. Time evolution of the gelation front x_g and the cracking front x_c, corresponding to the experiment shown in Fig. 4. At $t=t_0$, the magnetic field is applied in the y direction and the position of the gelation front is $x_g=x_H$. At $t=t_1$, the cracking front reaches the position $x_c=x_H$. We notice that the distance $d=x_g-x_c$ is constant for $x_c<x_H$.

For $t>t_1$, the cracks turn to align in the direction of the applied magnetic field. We notice that the line $x=x_H$ remains white on the images for $t>t_0$. This effect is probably due to a variation of the thickness of the gel phase when the magnetic field is suddenly changed.

Figure 6 represents the time evolution of the position of the gelation front x_g and the cracking front x_c, corresponding to Fig. 5. The gelation front propagates at a constant velocity independently of the presence of an external magnetic field. The effect of the magnetic field has a pronounced influence on the dynamics of the cracking front: it propagates at the same constant velocity as the gelation front for $t<t_1$ and slows down at $t>t_1$.

The experiment corresponding to Figs. 6 has been reproducibly performed several times using the same ferrofluid and the same experimental conditions.

The magnetic field has only an effect on the crack orientation if the cracks propagate in a gel that has been gelified with being exposed to a magnetic field. This fact is nicely illustrated by the experiment presented in Fig. 7, which shows the final stage of a ferrofluid drop which dried under the effect of a magnetic field applied during a short period only (corresponding to $x_1<x_g<x_2$): the cracks turn toward the direction of the field in the region $x_1<x<x_2$ and propagate radially for $x<x_1$ and for $x>x_2$, where the gel has been formed with no applied magnetic field. The gel phase therefore keeps a memory of the presence or absence of an external magnetic field during the gel formation. This memory effect can be accounted for by the presence of additional magnetic stresses within the gel phase formed under the effect of $\vec{H}$. The cracks are sensitive to these additional anisotropic stresses, which tend to align the cracks in the same direction as the external field and compete with the elastic stresses. On the contrary, when the gel is formed without a magnetic field ($x<x_1$ and $x>x_2$ in Fig. 7 or $x<x_H$ in Fig. 5), the magnetic dipoles are randomly oriented in the gel phase. Therefore, no magnetic stress exists in the gel phase, which behaves as a nonmagnetic colloidal gel, even if a magnetic field is applied to the gel.

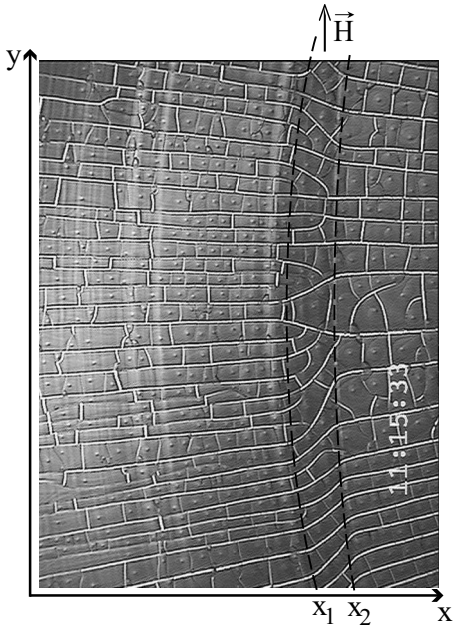

FIG. 7. Image of a region of a fully dried ferrofluid drop. The x axis represents the direction of propagation of the gelation front during the drying. An external magnetic field $H=25$ kA m^{-1} was applied in the y direction for the position of the gelation front $x_1<x_g<x_2$. The crack trajectories are bent toward the y direction only within the region that gelified while being exposed to the magnetic field.

V. THEORETICAL MODEL

In this section, we first recall the main theoretical description of crack formation induced by the drying process in nonmagnetic colloids, based on Ref. [4]. We then introduce the effect of additional magnetic stresses acting on the crack in the case of a drying ferrofluid droplet. We then compute the crack shape and compare the model to the experimental data.

The geometry considered here is a drop lying on a solid substrate, the upper surface being a free surface. In the plane of the substrate, the gelation front and the cracking front are assumed to be straight lines parallel to the y axis and propagating linearly in the x direction. This geometry represents the experimental situation where a surface of the order of 100 μm$\times$100 μm is considered, which corresponds to approximately 0.01% of the total surface of the drop. The thickness h of the gel phase is assumed to be homogeneous, which is well confirmed experimentally.

A. Crack pattern in the absence of a magnetic field

Within the gel phase, the equilibrium profile of the solvent volume fraction behind the gelation front can be computed taking into account the solvent evaporation at the free surface of the drop and the diffusion of solvent within the gel (see Fig. 8 for the notation). During solvent evaporation, the variation of solvent volume leads to a shrinkage of the gel phase. Because of the adhesion of the gel on the substrate, a tensile stress builds up in the gel.

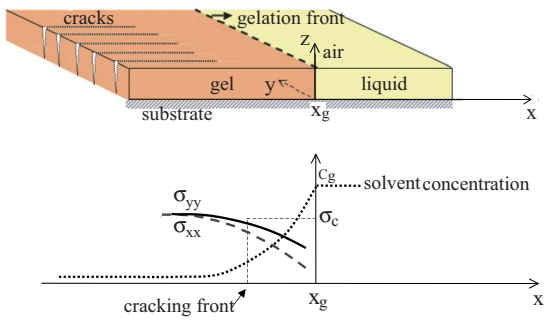

FIG. 8. (Color online) Three-dimensional sketch of a drying colloidal suspension. The gel phase of the drop is assumed to have a constant thickness h. Here, the liquid phase is also represented flat for simplicity, but this is not necessary for the presented model. $x=x_g$ corresponds to the position of the gelation front, which propagates in the direction $x>x_g$. At $z=0$, the drop lies on the substrate and the free surface between the drop and the air is at height $z=h$. Below the sketch, the variation of the two-dimensional (2D) solvent volume fraction $\bar{c}$ and the principal components of the 2D elastic stress tensor are plotted versus x.

Figure 8 shows the components of the two-dimensional stress tensor $\vec{\vec{\sigma}}$ in the (x,y) plane, obtained by averaging the three-dimensional stress tensor $\vec{\vec{\Sigma}}(x,y,z)$ of the gel phase along the gel thickness (see Appendix A for detailed calculations). The sketch in Fig. 8 shows the principal components σ_{xx} and σ_{yy} as a function of x in the gel phase $(x<x_g)$, showing that the elastic stress increases when x decreases. The problem is assumed to be invariant in the y direction.

According to Griffith's theory [19], the limit stress σ_c beyond which the material ruptures is a function of the stress intensity factor K_{IC} and is expressed as $\sigma_c=K_{IC}/\sqrt{\pi b}$, where b is a minimal characteristic size of the crack (of the order of the particle radius a) and K_{IC} depends on the physicochemistry of the gel phase. Thus, a crack forms when

$$\sigma_{nn} = \vec{n} \cdot (\vec{\vec{\sigma}}\vec{n}) = \sigma_c, \tag{1}$$

where σ_{nn} is the stress in the direction $\vec{n}$, normal to the crack. Equation (1) can be expressed as a function of the principal components of the stress tensor: $\sigma_{nn}=\sigma_{xx}\sin^2\theta+\sigma_{yy}\cos^2\theta$, where θ is the angle between $\vec{n}$ and the y axis.

Since in our geometry $\sigma_{yy}>\sigma_{xx}$ (Fig. 8), σ_{yy} reaches σ_c at a shorter distance from the gelation front than σ_{xx}. Cracks form and propagate in the x direction in order to relax σ_{yy}. The length over which σ_{yy} increases and reaches σ_c fixes the distance, $d=x_g-x_c$, between the gelation front and the cracking front (Fig. 6). d can be computed using Eqs. (1) and (B7) taking into account Appendix B:

$$\sigma_{yy} = \sigma_c \Rightarrow \frac{Ec_g}{1-2\nu}(1-e^{-d/\xi}) = \sigma_c, \tag{2}$$

where E is the Young's modulus of the gel phase when cracks form, ν is the Poisson ratio, c_g denotes the volume fraction of solvent at the gelation front, and $\xi=hv/J_E$ is a characteristic diffusion length defined from the thickness of the gel layer, h, the speed of the gelation front, v, and the evaporation rate J_E of the solvent in the air which mainly depends on the ambient relative humidity (see Appendix A).

B. Cracks oriented by the magnetic field in a magnetic gel

If no magnetic field is applied during the gel formation, the magnetic particles are randomly oriented and the colloid behaves like a nonmagnetic colloid. In contrast, if a magnetic field is applied, the magnetic dipoles align during the gelification. Once gelified, the magnetic particles are closely packed: their translational or rotational movement is obstructed—even after the magnetic field is removed. Therefore, the regions that have been gelified under the effect of a magnetic field have a permanent nonzero magnetization M^*.

Neglecting superparamagnetic effects (rotation of the magnetic moment of a particle with no particle rotation) and thermal agitation in the gel phase, the permanent magnetization of the gel is given by

$$M^* = M(H)\frac{V_{FF}}{V_{gel}} = \frac{\chi H}{\phi_{FF}}(1-\bar{c}), \tag{3}$$

where $M(H)$ is the ferrofluid magnetization corresponding to the value of H applied during the gelation [Fig. 4(b)]: for $H\leq 25$ kA m^{-1}, $M=\chi H$, where χ is the ferrofluid magnetic susceptibility. V_{FF} is the ferrofluid volume before drying, V_{gel} is the volume of the gel, ϕ_{FF} is the initial volume fraction of particles in the ferrofluid, and $\bar{c}$ is the water volume fraction of the gel phase averaged along the layer thickness $(1-\bar{c}$ is therefore the particle volume fraction in the gel). We assume that $M(H)$ is homogeneous in the ferrofluid. However, since $\bar{c}$ depends on x, M^* depends on x. In the referential of the gelation front $x'=x-vt$, $\bar{c}(x')$ is static; therefore, $M^*(x')$ does not depend on time. $M^*(x')$ is the permanent magnetization of the gel phase even in the absence of an external applied field.

In the following, we consider that the gel has been formed under the effect of the external magnetic field $\vec{H}$ and that H has been set to zero after the gel formation and before the crack propagation. We then describe the crack propagation in a magnetic gel of permanent magnetization M^* with no external magnetic field.

In the so-formed magnetic gel phase, the particles interact via anisotropic magnetic-dipole interactions, which are attractive if the particles are aligned along chains and repulsive if the particles are side by side. When a crack propagates, the crack opens a region filled with air, which splits the space into two regions made of the magnetic gel. Those two regions interact because of the magnetic-dipole interaction. The magnetic force exerted by one region on the second one can be computed. We note with index 1 or 2 the parameters that are defined in the first or second region separated by the crack (see Fig. 9).

Let $\vec{H}_1$ be the internal magnetic field induced by the magnetic moments present in the semispace 1 of volume V_1. $\vec{H}_1$ can be written as the gradient of a potential function [15]:

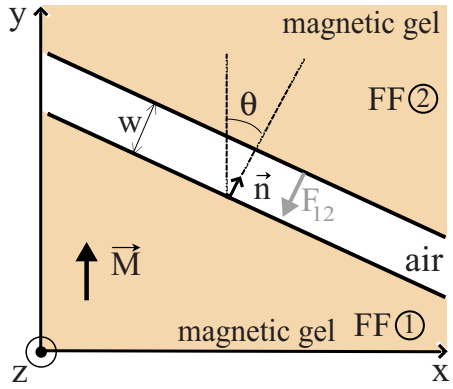

FIG. 9. (Color online) Notation for the calculation of the magnetic stress. The crack (width w) splits the (x,y) plane between two regions. M^* is the permanent magnetization of the magnetic gel. n is the normal to the crack interface of the semispace 1, θ is the angle between M^* and n, and F_{12} is the magnetic force exerted by region 1 onto region 2.

$$\vec{H}_1 = \vec{\nabla}\Psi_1, \tag{4}$$

with

$$\Psi_1(\vec{r}) = \frac{\mu_0}{4\pi}\int_{V_1}(\vec{M}^*\cdot\vec{\nabla})\frac{d^3\vec{\rho}}{\|\vec{r}-\vec{\rho}\|} = -\frac{\mu_0}{4\pi}\int_{S_1}(\vec{M}^*\cdot\vec{n})\frac{d^2\vec{\rho}}{\|\vec{r}-\vec{\rho}\|},$$

where $\vec{r}$ and $\vec{\rho}$ denote the dipole positions in three-dimensional space, S_1 is the surface enclosing the volume of V_1 region 1, and $\vec{n}$ is a unit vector normal to the external boundary of the volume V_1. In the cracked region, $\vec{n}$ is then normal to the crack, directed from region 1 to region 2. Therefore, the magnetic force exerted by region 1 on region 2 results from the interaction between the magnetic dipoles in the volume V_2 and the magnetic field $\vec{H}_1$ calculated above:

$$\vec{F}_{12} = \int_{V_2}(\vec{M}^*\cdot\vec{\nabla})\vec{H}_1 d^3\vec{r},$$

$$\vec{F}_{12} = -\frac{\mu_0}{4\pi}(\vec{M}^*\cdot\vec{n})^2\int_{S_2}d^2\vec{r}\int_{S_1}d^2\vec{\rho}\frac{(\vec{r}-\vec{\rho})}{\|\vec{r}-\vec{\rho}\|^3}, \tag{5}$$

where S_2 is the surface enclosing the volume V_2. The integration can then be performed, assuming that regions 1 and 2 are two semi-infinite regions in the x and y directions. After some calculation, we obtain

$$\vec{F}_{12} = -\frac{\mu_0}{\pi}(M^*\cos\theta)^2 L\left\{h\arctan\left(\frac{h}{w}\right) - w\ln\left[1+\left(\frac{h}{w}\right)^2\right]\right\}\vec{n},$$

where w is the width and L is the length of the crack. In the limit of a thin crack $(w \ll h)$, we find

$$\vec{F}_{12} = -\frac{\mu_0}{2}(M^*\cos\theta)^2 Lh\vec{n}, \tag{6}$$

where θ is the angle between $\vec{n}$ and $\vec{M}^*$. Therefore, the effect of the force is to close the crack when $\theta \neq \pi/2$—i.e., when the crack is not parallel to the magnetization.

Equation (6) is independent of the crack width w and varies linearly with the crack length L. Therefore, it can be used to define a magnetic stress σ_m which will affect the crack propagation:

$$\vec{F}_{12} = -Lh\sigma_m\vec{n}, \tag{7}$$

where

$$\sigma_m = -\frac{\mu_0}{2}M^{*2}\cos^2\theta. \tag{8}$$

Under the effect of the external magnetic field, the condition for the crack formation [Eq. (1)] becomes $\sigma_{nn}+\sigma_m=\sigma_c$, which can be written in the following way:

$$\sigma_{nn} = \sigma_c - \sigma_m = \sigma_c + \frac{\mu_0}{2}M^{*2}\cos^2\theta. \tag{9}$$

Equation (9) shows that the effect of the magnetic-dipole interactions is to increase the critical stress above which the crack propagates. However, this effect is anisotropic. To illustrate this effect, let us consider those two extreme cases. For $\theta=0$, the cracks will form perpendicularly to the magnetization if, according to Eq. (9),

$$\sigma_{yy}(\theta=0) = \sigma_c + \frac{\mu_0}{2}M^{*2}. \tag{10}$$

For $\theta=\frac{\pi}{2}$, the cracks will align in the direction of the magnetization if

$$\sigma_{x'x'}\left(\theta=\frac{\pi}{2}\right) = \sigma_c. \tag{11}$$

The total critical stress $\sigma_c+\sigma_m$ is then increased by the existence of a permanent magnetization in the case $\theta=0$, whereas it is not affected by M^* in the case $\theta=\frac{\pi}{2}$. Therefore (see Fig. 8), if M^* is strong enough, the distance from the gelation front at which $\sigma_{x'x'}=\sigma_c$ is smaller than the distance at which $\sigma_{yy}=\sigma_c+\sigma_m$, the cracks turn in the direction that relaxes $\sigma_{x'x'}$—i.e., in the direction of the magnetic field applied during the gel formation. However, this argument shows that there is a critical value of M^* above which the crack can change orientation.

Equation (9) gives the value of the angle θ of maximum total stress. In order to compute the shape of the crack trajectory, we have to solve the following set of differential equations:

$$\frac{dx'}{dl} = \cos\theta, \quad \frac{dy}{dl} = \sin\theta, \tag{12}$$

where l denotes the arclength along the crack. The computed crack shape can then be compared to the experimental data, as presented in the following section.

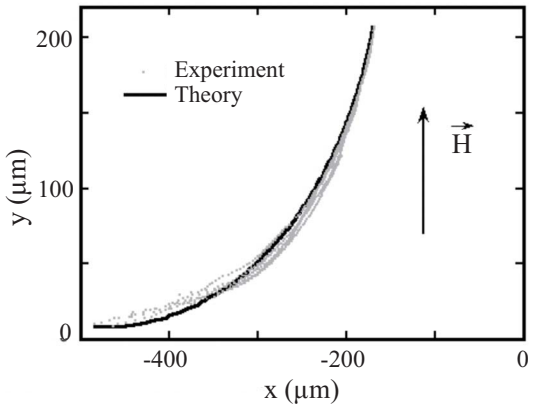

FIG. 10. (Color online) Trajectory of the curved crack under the effect of the external magnetic field, applied in the y direction, of amplitude $H=16$ kA m^{-1}. The x axis is the direction of propagation of the gelation front during the drying in the referential of the laboratory. The dots represent the experimental data. They correspond to the shape of eight primary cracks, translated in the x and y directions or symmetrized with respect to the y axis. The solid line is a fit of the data using the model presented in Sec. V. $x=0$ corresponds to the position of the gelation when the crack is aligned in the direction of the magnetic field.

VI. COMPARISON BETWEEN THE THEORETICAL MODEL AND THE EXPERIMENTAL DATA

Figure 10 shows the comparison between the experimental data and the model described above. The data represent the shape of a crack in the (x,y) plane, or equivalently the trajectory of a crack, in a region that has been gelified under the effect of $\vec{H}$. The crack propagated in time in the x direction. The crack shape is plotted in the referential of the laboratory, the origin $x=0$ corresponding to the position of the gelation front when the crack is aligned in the direction of the field $[\sigma_{xx}(x=0)=\sigma_{yy}(x=0)=0]$.

In Fig. 10, the experimental data represent eight different cracks. The cracks, slightly translated in the y and x directions, or symmetrized with respect to the y axis (but not dilated in any direction), collapse on the same master curve: the crack shape is reproducible and can therefore be compared to the theoretical model.

Let us notice that only the primary cracks have been considered—i.e., the cracks that propagate in a gel free of cracks. The secondary cracks explore a gel where a crack has already propagated; therefore, the stress field is modified by the presence of the primary crack. The model presented here does not consider the secondary cracks. Figure 10 corresponds to the same experimental conditions as in Fig. 1 (same amplitude of the magnetic field), where many primary cracks are visible. In Fig. 5(c), most of the cracks are secondary cracks since they end up meeting a primary crack with a 90° angle. The interactions between cracks seem stronger in the case of Fig. 5, which also corresponds to a larger amplitude of the magnetic field than in Fig. 1. Since the model only considers the shape of the primary case, we have chosen a situation close to the case of Fig. 1.

The solid line in Fig. 10 corresponds to the model presented in Sec. V. Equations (2), (9), (12), and (B7) lead to the following expression used for the fit:

$$\sin^2\theta = \frac{1-\dfrac{1-\exp(x/\xi)}{1-\exp(-d/\xi)}+\dfrac{\mu_0 M^{*2}}{2\sigma_c}}{1-\dfrac{\exp(x/\xi)-\exp(\alpha x)}{[1-\exp(-d/\xi)][1-(\alpha\xi)^2]}+\dfrac{\mu_0 M^{*2}}{2\sigma_c}}. \tag{13}$$

The parameters of Eq. (13) are set as follows: the distance d between the gelation front and the cracking front when $H=0$ is measured for $H=16$ kA m^{-1}: $d=140$ μm.

The gel thickness is assumed to be homogeneous and is inferred from the data: $h=100$ μm. For this thickness and under an ambient relative humidity of 50%, the evaporation rate can be calculated numerically [18]: $J_E=2\times10^{-6}$ m s^{-1}. The velocity of the gelation front is constant (see Fig. 6). For $H=16$ kA m^{-1}, we measure: $v=10$ μm s^{-1}. Therefore, $\xi=hv/J_E=500$ μm. Those values of h and ξ are coherent with the theory presented above. Indeed, let d_H be the distance between the gelation front and the cracking front when $H\neq0$, after the crack has turned in the direction of the magnetic field. Equations (11) and (B7) give the following condition for d_H:

$$\frac{Ec_g}{1-2\nu}\left(\frac{\exp(-d_H/\xi)-\exp(-\alpha d_H)}{1-(\alpha\xi)^2}+[1-\exp(-d_H/\xi)]\right)=\sigma_c.$$

Therefore, according to Eq. (2),

$$\frac{\exp(-d_H\xi)-\exp(-\alpha d_H)}{1-(\alpha\xi)^2}=\exp(-d_H/\xi)-\exp(-d/\xi).$$

For $H=16$ kA m^{-1}, we measure $d_H=170$ μm. We find that this value satisfies very well the above equation. This justifies *a posteriori* the choice $h=100$ μm.

The Poisson ratio is set to $\nu=0.3$, which is the usual value of the Poisson ratio of a colloidal gel [4].

The crack shape is then calculated and plotted with one fitting parameter. The best fit, plotted in Fig. 10, gives

$$\frac{M^{*2}}{\sigma_c}=2.43\times10^6 \text{ A}^2\text{ m}^{-2}\text{ Pa}^{-1}. \tag{14}$$

This result allows us to obtain an order of magnitude of the gel Young's modulus just before the crack propagation. The magnetization of the gel at the tip if the crack is given by Eqs. (3) and (A2): $M^*=\frac{\chi H}{\phi_{FF}}(1-c_g e^{-d_H/\xi})\sim77$ kA m^{-1}, where the volume fraction of solvent in the ferrofluid at the gelation front is set to $c_g\sim0.9$. Therefore, according to Eq. (2), the Young's modulus can be estimated. We obtain $E\sim4\times10^3$ Pa.

VII. DISCUSSION

The value of the gel Young's modulus E obtained above is two orders of magnitude lower than the results of the mea-

surements performed by Zarzycki for a wet silica gel [20]. This effect could be due to several factors. First, the method presented here gives an estimation of the gel Young's modulus just before the crack propagation, whereas direct measurements of Ref. [20] are performed in a drier gel (Ludox SM with average particle diameter ~15 nm), in which the solvent evaporation leads to an increase of the gel elastic modulus. It is then reasonable to expect a lower value in our case that is in a region of the gel which is consolidating. In addition, the magnetization of the gel seems to be undervalued here: its value could be higher in the crack tip, which has not been considered here.

Another effect could be due to the magnetic-dipole interaction, which could lead the formation of chains of magnetic particles in the direction of the applied field during the drying. This would therefore fragilize the gel in the perpendicular direction and then lower the value of the elastic Young's modulus. In order to test this hypothesis, it would be interesting to perform direct measurements of the Young's modulus of the magnetic gel and to compare the case of a gel formed under the effect of a magnetic field and the case of a gel formed with no applied field.

However, the model presented above is very simplified. In particular, the main approximations are the hypothesis of a homogeneous thickness and the assumption of an isotropic material. This model captures the fact that the crack rotation is due to the magnetic-dipole interaction and gives an estimate of the order of magnitude of the gel Young's modulus before the crack propagation. In order to use this method to actually measure the gel Young's modulus, a more precise model is required, which would take into account the effects of a heterogeneous thickness and of anisotropy.

VIII. CONCLUSION

In this article, we have shown that the morphology of cracks in a drying ferrofluid droplet can be controlled by an external magnetic field applied during the gel formation. This effect is due to the building up of internal magnetic stresses in the gel, which remain in the gel even when the magnetic field is removed. These stresses compete with the elastic stresses and tend to align the crack in the direction of the internal gel magnetization. The analysis of the shape of the crack allows one then to obtain an estimate of the gel Young's modulus.

However, experiments performed using different ferrofluids have shown that the drying pattern can be very different from one ferrofluid to another one. This does not seem to be due to the nature of the magnetic particles (we obtained patterns similar to the ones shown in this article using a ferro-fluid made of cobalt ferrite particles), but rather to the nature of the ions and counter-ions used to stabilize the colloid. Indeed, the phase diagram of magnetic liquid colloidal suspensions is extremely rich [14] and the crack pattern obtained during the drying of a ferrofluid drop might strongly depend on the path followed in the phase diagram. A complete physicochemical study of this effect is still to be done.

ACKNOWLEDGMENTS

We would like to thank Dr. E. Dubois for enlightening discussions and for the magnetization curve of the ferrofluid. We thank Dr. W. Drenckhan for fruitful discussions. L.P. acknowledges support by the project ANR-05-JCJC-0029.

APPENDIX A: WATER VOLUME FRACTION IN THE DRYING GEL WITHOUT A MAGNETIC FIELD

Let us consider the fracture-free area between the cracking front and the gelation front (see sketch in Fig. 8). In this region, the stress distribution is related to the diffusive volume fraction field c of the solvent. Since the solvent evaporates from the gel surface—that is, at $z=h$—c is both x and z dependent. Also, the solvent flow in the gel phase is driven by the capillary pressure gradients arising due to the curvature of the capillary bridges between the particles. This flow has a volume flux of the solvent $\vec{J}_v \simeq -r^2 \vec{\nabla} p_c / \eta$. Since the capillary pressure is $p_c = -\sigma / r$ and at small volume fraction of the liquid $c \simeq r/R$, where r is the curvature radius of the capillary bridge and R is the radius of the colloidal particles, we have $\vec{J}_v = -D_g \vec{\nabla} c$, where the diffusion coefficient of the solvent, which is related to the transport of solvent through the porous solid gel, is $D_g = R^2/\tau$ and τ is characteristic capillary relaxation time of the bridge $\tau \simeq \eta R/\sigma$. Then mass conservation is expressed as

$$\frac{\partial c}{\partial t} = -\operatorname{div} \vec{J}_v.$$

In the following, we will consider the steady-state solution $c = c(x - vt)$ in the case of the constant gelation front velocity after averaging the volume fraction of the solvent along the vertical z in the region $z \leq h$—that is, $\bar{c}$. In that way,

$$-v \frac{\partial \bar{c}}{\partial x'} = D_g \frac{\partial^2 \bar{c}}{\partial x'^2} + \left. \frac{J_E \bar{c}}{h} \right|_{z=h}. \tag{A1}$$

In analogy to Newton's law for cooling at the interface of the film,

$$-D_g \left. \frac{\partial c}{\partial z} \right|_{z=h} = J_E \bar{c}.$$

J_E is determined by the solvent diffusion in the vapor phase and depends on the external conditions. Hence, the solvent transfer in the gel satisfies a diffusion equation, which we denote in a moving coordinate system x', y, z attached to the gelation front, moving at velocity v.

The term $D_g \left(\frac{\partial c}{\partial z}\right)_{z=h}$ is related to the evaporation rate at the gel-air interface. The solution of Eq. (A1) in the gel phase $(x' \leq 0)$ at $D_g J_E / (hv^2) \ll 1$ is

$$\bar{c}(x') = c_g e^{x'/\xi}, \tag{A2}$$

where $\xi = hv/J_E$ is a characteristic diffusion length and c_g denotes the volume fraction of solvent at the gelation front.

APPENDIX B: INTERNAL STRESS IN THE DRYING GEL WITHOUT A MAGNETIC FIELD

Let us compute the elastic stress within the gel in the referential attached to the gelation front. Assuming that the material is both isotropic and homogeneous, the classical theory of elasticity is applicable [21]. The components of the stress tensor are given by

$$\Sigma_{ij} = \frac{E}{1+\nu}\left(u_{ij} + \frac{\nu}{1-2\nu}\delta_{ij}u_{ll}\right) + \frac{E}{1-2\nu}\delta_{ij}(c_g - c), \tag{B1}$$

where $i,j=x',y,z$. The second term on the right-hand side is the internal stress created by the variations of the solvent volume fraction, c_g-c. In Eq. (B1), the evolution of the solvent volume fraction is treated by analogy to temperature variations in a nonisothermal problem. $u_{ij}=\frac{1}{2}(\partial_i u_j+\partial_j u_i)$ represents the components of the deformation tensor with respect to the components of the displacement field, u_i, within the gel.

The displacement field is of the form $\vec{u}=(u_{x'}(x',z),0,0)$. Equation (B1) gives the following expressions for the nonzero components of the stress tensor:

$$\Sigma_{x'x'} = \frac{E(1-\nu)}{(1+\nu)(1-2\nu)}\frac{\partial u_{x'}}{\partial x'} + \frac{E}{1-2\nu}(c_g - c) \tag{B2}$$

and

$$\Sigma_{x'z} = \frac{E}{2(1+\nu)}\frac{\partial u_{x'}}{\partial z}. \tag{B3}$$

The boundary conditions are $u_{x'}(x',y,z=0)=0$ (no slip on the substrate) and $\Sigma_{x'z}(x',y,z=h)=0$ (free surface at the gel-air interface). They are satisfied using $u_{x'}(x',y,z)=F(x')\sin(\pi z/2h)$, where $F(x')$ is a function of x', which we calculate now. The condition of mechanical equilibrium of the gel is [21,22]

$$\frac{\partial \Sigma_{x'x'}}{\partial x'} + \frac{\partial \Sigma_{x'z}}{\partial z} = 0. \tag{B4}$$

We define the components of the stress tensor averaged along the gel thickness with respect to z:

$$\sigma_{ij} = \frac{1}{h}\int_0^h \Sigma_{ij} dz, \tag{B5}$$

with $i,j=x',y,z$. Using Eqs. (B4) and (B5) and the boundary condition at the free interface, we obtain

$$\frac{\partial \sigma_{x'x'}}{\partial x'} - \frac{1}{h}\Sigma_{x'z}\bigg|_{z=0} = 0. \tag{B6}$$

The function $F(x')$ is then determined using Eqs. (A2), (B2), and (B6) and the boundary condition of vanishing stress on the gelation front, $\sigma_{x'x'}(x'=0,y)=0$:

$$F(x') = \frac{\pi(1+\nu)c_g}{2(1-\nu)\xi}\frac{\exp(x'/\xi) - \frac{1}{\alpha\xi}\exp(\alpha x')}{1/\xi^2 - \alpha^2},$$

where

$$\alpha^2 = \left(\frac{\pi}{2h}\right)^2 \frac{(1-2\nu)}{2(1-\nu)}.$$

Therefore, the z-averaged stress distribution in the gel is

$$\sigma_{x'x'} = \frac{Ec_g}{1-2\nu}\frac{\exp(x'/\xi) - \exp(\alpha x')}{1-(\alpha\xi)^2} + \sigma_{yy},$$

$$\sigma_{yy} = \frac{Ec_g}{1-2\nu}[1 - \exp(x'/\xi)]. \tag{B7}$$

[1] H. Colina and S. Roux, Eur. Phys. J. E **1**, 189 (2000).
[2] A. Toussaint, Prog. Org. Coat. **2**, 237 (1974).
[3] A. Goldsworthy, *Time* (Anthèse, Arcueil, France, 2002). A piece of art presented in this book (picture on the front page) consists in orienting the cracks induced by the drying of a mud spread on the internal wall of a church. The orientation of the cracks is a result of a subtle choice of materials incorporated into the mud before the drying.
[4] C. J. Brinker and G. W. Scherer, *Sol-Gel Science: The Physics and Chemistry of Sol Gel Processing* (Academic, San Diego, 1990).
[5] P. S. Plummer and V. A. Gostin, J. Sediment. Petrol. **51**, 1147 (1981).
[6] A. Atkinson and R. M. Guppy, J. Mater. Sci. **26**, 3869 (1991); A. Groisman and E. Kaplan, Europhys. Lett. **25**, 415 (1994).
[7] C. Allain and L. Limat, Phys. Rev. Lett. **74**, 2981 (1995).
[8] L. Pauchard, F. Parisse, and C. Allain, Phys. Rev. E **59**, 3737 (1999).
[9] E. R. Dufresne, E. I. Corwin, N. A. Greenblatt, J. Ashmore, D. Y. Wang, A. D. Dinsmore, J. X. Cheng, X. S. Xie, J. W. Hutchinson, and D. A. Weitz, Phys. Rev. Lett. **91**, 224501 (2003).
[10] A. Yuse and M. Sano, Nature (London) **362**, 329 (1993).
[11] S.-I. Sasa, K. Sekimoto, and H. Nakanishi, Phys. Rev. E **50**, R1733 (1994).
[12] A. Nakahara and Y. Matsuo, J. Phys. Soc. Jpn. **74**, 1362 (2005).
[13] G. W. Scherer, J. Non-Cryst. Solids **144**, 210 (1992).
[14] F. Cousin, E. Dubois, and V. Cabuil, Phys. Rev. E **68**, 021405 (2003).
[15] E. Blums, A. Cebers, and M. M. Maiorov, *Magnetic Fluids* (de Gruyter, New York, 1997).
[16] R. E. Rosensweig, *Ferrohydrodynamics* (Dover, Mineola, NY, 1999).
[17] E. Lemaire and G. Bossis, J. Phys. D **24**, 1473 (1991).
[18] R. Deegan *et al.*, Nature (London) **389**, 827 (1997).
[19] A. A. Griffith, Philos. Trans. R. Soc. London, Ser. A **221**, 163 (1921).
[20] J. Zarzycki, J. Non-Cryst. Solids **100**, 359 (1988).
[21] L. Landau and E. M. Lifshitz, *Theory of Elasticity*, 3rd ed. (Pergamon Press, New York, 1986).
[22] L. Landau and E. M. Lifshitz, *Theory of Electrodynamics of Continuous Media* (Pergamon Press, New York, 1960).